SPE-204197-MS

# Modeling Multistage Acid Fracturing Treatments In Carbonate Reservoirs

Rencheng Dong and Mary F. Wheeler, The University of Texas at Austin; Hang Su, China University of Petroleum (Beijing); Kang Ma, CNOOC Research Institute Co., Ltd.



This paper was prepared for presentation at the SPE Hydraulic Fracturing Technology Conference and Exhibition held in Woodlands, Texas, USA, 2021.



## Abstract

As our industry is tapping into tighter carbonate reservoirs than in the past, completion techniques need to be improved to stimulate the low-permeability carbonate formation. Multistage acid fracturing technique has been developed in recent years and proved to be successful in some carbonate reservoirs. A multistage acid fracturing job is to perform several stages of acid fracturing along a horizontal well. The goal of acid fracturing operations is to create enough fracture roughness through differential acid etching on fracture walls such that the acid fracture can keep open and sustain a high enough acid fracture conductivity under the closure stress. In multistage acid fracturing treatments, acid flow is in a radial flow scenario and the acid etching process can be different from acid fracturing in vertical wells. In order to accurately predict the acid-fracture conductivity, a detailed description of the rough acid-fracture surfaces is required. In this paper, we developed a 3D acid transport model to compute the geometry of acid fracture for multistage acid fracturing treatments. The developed model couples the acid fluid flow, reactive transport and rock dissolution in the fracture. We also included acid viscous fingering in our model since viscous fingering mechanism is commonly applied in multistage acid fracturing to achieve non-uniform acid etching. Our simulation results reproduced the acid viscous fingering phenomenon observed from experiments in the literature. During the process of acid viscous fingering, high-conductivity channels developed in the fingering regions. We modeled the acid etching process in multistage acid fracturing treatments and compared it with acid fracturing treatments in vertical wells. We found that due to the radial flow effect, it is more difficult to achieve non-uniform acid etching in multistage acid fracturing treatments than in vertical wells. We investigated the effects of perforation design and pad fluid viscosity on multistage acid fracturing treatments. We need to have an adequate number of perforations in order to develop non-uniform acid etching. We found that a higher viscosity pad fluid helps acid to penetrate deeper in the fracture and result in a longer and narrower etched channel.

## Introduction

Since carbonate rock is very reactive, acid stimulation operations are widely performed in carbonate reservoirs to enhance the production of oil and gas. There are two main types of carbonate acid stimulation methods: (1) matrix acidizing and (2) acid fracturing [1]. The main difference between these two acid stimulation methods is the acid injection pressure. In matrix acidizing operations, the acid injection

pressure is lower than the formation fracture pressure while the acid injection pressure is higher than the formation fracture pressure in acid fracturing operations.

Matrix acidizing mainly stimulates the carbonate formation near the wellbore. As shown in **Fig. 1a**, formation damage usually occurs in the near-wellbore area. The matrix acidizing treatment is to inject the acid to dissolve the carbonate rock. As shown in **Fig. 1b**, a successful acidizing job can create high-conductivity channels, as known as wormholes, to remove formation damage. The wormhole growth has been studied through both experiments [2] and modeling [3, 4].


**Figure 1: Illustration of matrix acidizing treatments**

Acid fracturing is similar to hydraulic fracturing [1] because both of them involve creating fractures. The main difference between acid fracturing and hydraulic fracturing is how the fracture conductivity is created. In hydraulic fracturing operations [5], the proppant is injected after the pad stage to keep the induced fracture open, as shown in **Fig. 2a**. In acid fracturing operations, a pad fluid is first injected to break down the formation and create an initial fracture. The acid is then injected after the pad stage to etch fracture surfaces. We expect the acid etching on fracture surfaces to be non-uniform so that rough fracture surfaces can be created, as illustrated in **Fig. 2b**. After acid injection, the acid fracture tends to be closed under the closure stress in the formation. But the acid fracture is expected to be partially open with the support of asperities on fracture surfaces, as demonstrated in **Fig. 2c**. Therefore the acid fracture conductivity is created by the residual fracture opening.

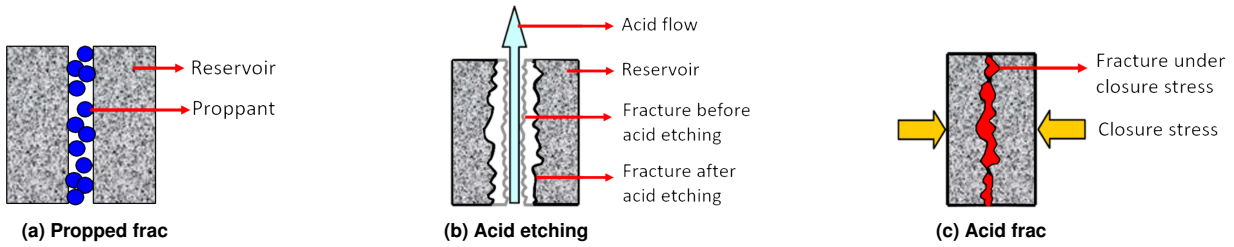


**Figure 2: Comparison of propped frac and acid frac**

In recent years, many carbonate reservoirs under development are tight formations [6, 7, 8]. The reservoir permeability is usually less than 10 mD. Acid stimulation methods need to be improved to tackle the challenges in low-permeability carbonate formations. One of the promising completion methods is the multistage acid fracturing technique in a horizontal well, illustrated in **Fig. 3**. This technique is similar to the multistage hydraulic fracturing technique which has been widely applied in developing shale reservoirs [9]. The horizontal well is usually drilled along the direction of minimum horizontal in-situ stress in the formation. Multiple stages of acid fracturing are planned along the horizontal well. For each stage, pad fluid is first injected to create a transverse fracture and then acid is injected to etch fracture surfaces. Recent field pilot tests have shown that multistage acid fracturing can substantially increase the production in low-permeability carbonate reservoirs [6, 7, 8].

The viscous fingering mechanism has been extensively utilized in multistage acid fracturing treatments to achieve non-uniform acid etching [6, 7, 8]. As shown in **Fig. 2b**, the key of creating acid fracture

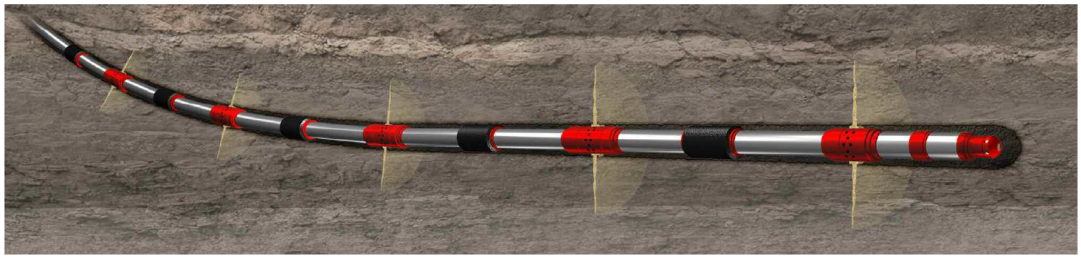

**Figure 3: Illustration of multistage acid fracturing in a horizontal well [6]**

conductivity is to have non-uniform or differential acid etching on fracture surfaces. Non-uniform acid etching can be induced by reservoir heterogeneity [10] and acid viscous fingering [11]. For heterogeneous reservoirs, different parts of fracture surfaces can have different reaction rates because they have different mineralogy. Therefore acid etching is non-uniform in heterogeneous reservoirs. For some relatively homogeneous reservoirs, non-uniform acid etching is usually enhanced by the viscous fingering technique. A typical pumping schedule in a vertical well is demonstrated in **Fig. 4a** [6]. A high-viscosity pad fluid is injected first to initiate and propagate the fracture. Afterwards a low-viscosity acid fluid is injected to displace the pad fluid. Since the acid fluid has a lower viscosity, acid viscous fingers will form in the fracture. More rocks are dissolved in the fingering regions than elsewhere. The acid viscous fingering has been observed in acid fracturing experiments, as shown in **Fig. 4b** [12]. Li et al. [12] used real rock as one fracture wall in their modified Hele-Shaw cell in order to introduce the dissolution reaction between acid and rock. In **Fig. 4b**, the acid fluid is dyed with a dark color and the polymer fluid is transparent. **Fig. 4b** shows that complicated acid fingering develops as acid displaces polymer and etches rock surface simultaneously.

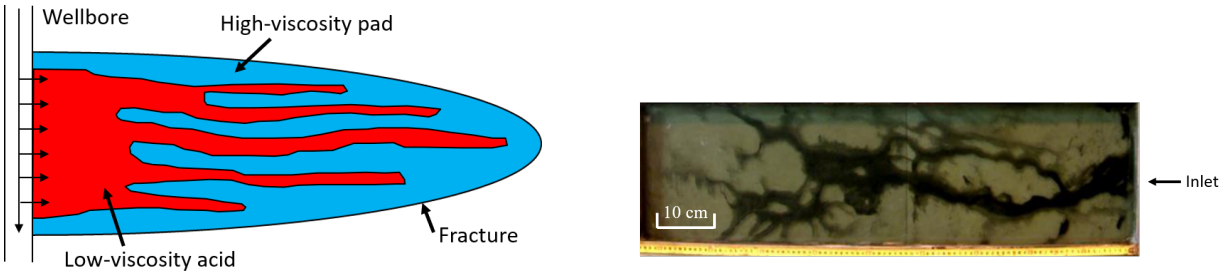


**(a) Acid viscous fingering technique [6]**

**(b) Acid viscous fingering in experiments [12]**

**Figure 4: Acid viscous fingering in acid fracturing**

Designing acid fracturing jobs requires understandings of how acid creates rough fracture surfaces to form acid fracture conductivity. Several models have been developed in the literature to account for the acid flow and reactive transport inside the fracture. Ben-Naceur and Economides [13] coupled an acid transport simulator with a 2D/pseudo 3D fracture model. They simulated both multi-stage injection treatments and gelled acid treatments. Similar to the K-factor theory [14], they developed a one-dimension fractional flow model to approximate the unstable flow due to acid viscous fingering. Gdanski and Lee [15] also developed an acid fracturing simulator which incorporated fracture geometry, temperature calculations and acid spending. Lo and Dean [16] modeled acid transport assuming an infinite reaction rate and coupled it with 2D fracture models. Settari [17] developed a comprehensive acid fracturing model that solved for 2D/pseudo 3D fracture geometry, leakoff, heat transfer and acid transport. This model accounted for multiple fluids, mass transfer controlled acidizing, reaction kinetics controlled acidizing, and leakoff due to wormholing in the matrix. Settari et al. [18] developed a 2D acid transport model which accounted for acid concentration along the fracture width direction. Romero et al. [19] developed a 3D

acid transport model and coupled it with a pseudo 3D hydraulic fracturing simulator. Previous work did not directly calculate the change of fracture geometry, especially the fracture width due to acid etching. Mou et al. [10] developed an intermediate-scale acid transport model which accounted for fracture face dissolution by acid. In this model, the fracture conductivity was calculated directly from rough acid-etched fracture surfaces. Li et al. [12] modeled acid fingering during acid fracturing. They did not consider the reaction between acid and carbonate rock in their model. In the geoscience community, mineral dissolution is also well studied since it is directly related to the formation of caves and karst. Starchenko et al. [20] developed a fracture dissolution simulator based on the OpenFOAM library [21]. They modeled flow, reactive transport inside the fracture and the change of fracture geometry. Starchenko and Ladd [22] studied different fracture dissolution regimes under different scenarios of flow and reactive transport through numerical simulations.

In the past, modeling studies of acid etching have been focusing on acid fracturing operations in vertical wells. Acid etching during multistage acid fracturing operations is rarely modeled. In the vertical well, acid flow is mostly along a single direction inside the fracture and usually named as linear flow. In the multistage acid fracturing, acid flow is radial flow inside the transverse fracture. Due to different flow regimes, acid etching in multistage acid fracturing can be different from that in vertical wells. An experimental apparatus was developed by Anderson and Fredrickson [23] to study acid etching under radial flow. The schematic of acid etching test cell is shown in **Fig. 5a**. For this type of acid etching test, a cylinder disk of rock sample needs to be prepared and a hole is drilled in the disk center. A metal plate is placed over the rock sample. The space between rock sample and the metal plate mimics a fracture. Acid is injected through the hole in the center of rock sample. Acid flows inside the fracture and etches the rock surface. An example of the acid etching test is shown in **Fig. 5b**. The experimental result showed that some dendritic etching patterns developed under the radial flow condition.

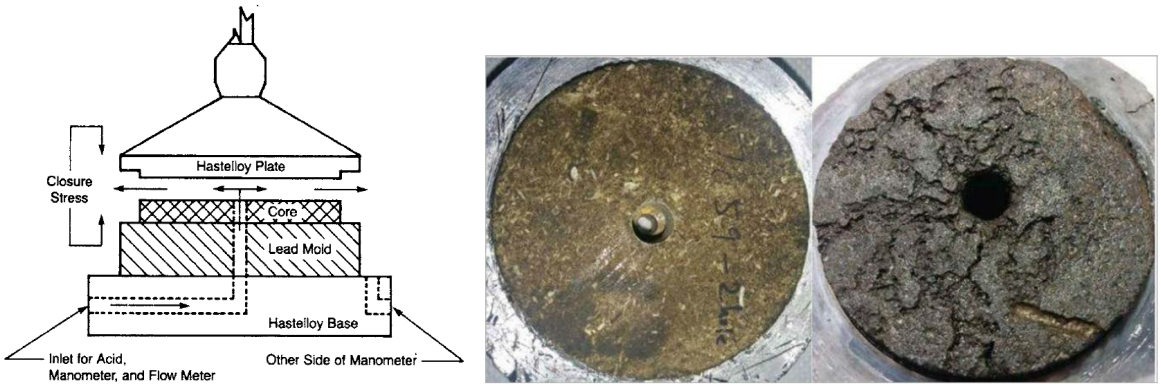


**(a) Acid etching test cell [23]** **(b) Carbonate before (left) and after (right) acid etching test [7]**

**Figure 5: Acid etching experiment under radial flow**

In this paper, we present a modeling study on acid etching process in multistage acid fracturing treatments. The focus of this paper is to investigate how to utilize non-uniform flow dynamics to achieve non-uniform acid etching. Therefore we also include acid viscous fingering in our model. Our mathematical model considers the following processes: (1) the fluid flow inside the fracture, (2) acid transport and polymer transport, (3) mineral dissolution at the fracture surface and (4) the change of fracture morphology. A numerical simulator has been developed based on the OpenFOAM library [21] to solve the mathematical model. We will study the effects of radial flow and acid viscous fingering on acid etching process through numerical simulations.

## Mathematical Model

The focus of this study is the acid injection period after a fracture has been created during the pad stage. The fracture is assumed not to propagate during the acid injection stage. The fracture domain in a vertical well is illustrated in **Fig. 6a** where the fracture width is exaggerated for the purpose of illustration. Six boundary faces are defined: (1) inlet, (2) outlet, (3) top face, (4) bottom face, and (5) two fracture wall faces. The mineral of the reservoir formation is calcite. The pad fluid is a polymer solution while the acid fluid is a hydrochloric acid (HCl) solution. The domain of a transverse fracture in multistage acid fracturing treatments is shown in **Fig. 6b**. Acid etching under the linear flow condition is modeled with the geometry in **Fig. 6a** while acid etching under the radial flow condition is modeled with the geometry in **Fig. 6b**. The inlet face in **Fig. 6b** represents a horizontal wellbore. The governing equations for describing acid etching process under both linear and radial flow scenarios are roughly the same except differences in boundary conditions. In this section, governing equations will be explained with respect to the geometry in **Fig. 6a**.

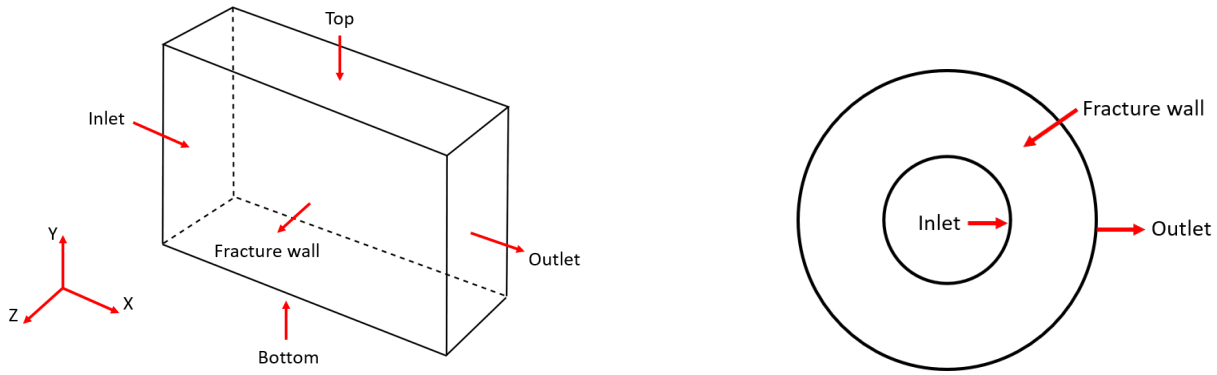


**(a) Fracture domain in a vertical well** **(b) Transverse fracture domain (gun-barrel view)**

**Figure 6: Schematics of fracture domains**

### Model Assumptions

1. Only aqueous phase fluid exists in the open fracture.
2. The aqueous phase fluid is incompressible Newtonian fluid with constant density.
3. Gravity is not considered.
4. The fluid flow in the fracture is laminar flow.
5. Acid leak-off from the fracture to the surrounding reservoir rock is ignored.

### Fluid Flow Model

The fluid flow model consists of the momentum equation and the continuity equation. The momentum equation is the incompressible Navier-Stokes equation as shown in **Eq. (1)**. Since the acid etching is slower than the fluid motion, the momentum equation is assumed to be steady-state for each time step. During the acid injection period, the velocity field still changes due to changes in fracture geometry and fluid composition.

$$\rho(\mathbf{u}\cdot\nabla\mathbf{u}) = -\nabla p + \mu\nabla^2\mathbf{u} \tag{1}$$

where $\rho$ is the fluid density, $\mathbf{u}$ is the fluid velocity, $p$ is the fluid pressure and $\mu$ is the fluid viscosity.

The continuity equation of the aqueous phase fluid is

$$\nabla\cdot\mathbf{u} = 0 \tag{2}$$

The velocity field $\mathbf{u}$ can be resolved by solving the coupled momentum equation **Eq. (1)** and continuity equation **Eq. (2)**.

The fluid flow model is closed by the following boundary conditions

$$\mathbf{u} = \mathbf{u}_{\text{inj}} \quad \text{inlet face} \tag{3}$$

$$p = p_{\text{out}} \quad \text{outlet face} \tag{4}$$

$$\mathbf{u} = 0 \quad \text{top/bottom/fracture wall faces} \tag{5}$$

A specific flow rate $\mathbf{u}_{\text{inj}}$ is maintained at the inlet boundary while a specific pressure $p_{\text{out}}$ is defined at the outlet boundary. No slip boundary conditions are applied at the other boundaries.

**Acid Transport Model**

Since the dissolution reaction rate depends on the proton ($H^+$) concentration, we need to track the $H^+$ concentration in the aqueous phase fluid. The acid transport is described by the following advection-diffusion equation

$$\frac{\partial c_1}{\partial t} + \nabla \cdot (\mathbf{u} c_1) - \nabla \cdot (\mathbf{D}_1 \nabla c_1) = 0 \tag{6}$$

where $c_1$ is the molar concentration of $H^+$ and $\mathbf{D}_1$ is the $H^+$ diffusion-dispersion coefficient.

The boundary conditions of the acid transport model are defined as below.

$$(\mathbf{u} c_1 - \mathbf{D}_1 \nabla c_1) \cdot \mathbf{n} = (\mathbf{u}_{\text{inj}} \cdot \mathbf{n}) c_1^{\text{inj}} \quad \text{inlet face} \tag{7}$$

$$-\mathbf{D}_1 \nabla c_1 \cdot \mathbf{n} = 0 \quad \text{outlet/top/bottom faces} \tag{8}$$

$$-\mathbf{D}_1 \nabla c_1 \cdot \mathbf{n} = R(c_1) \quad \text{fracture wall faces} \tag{9}$$

where $\mathbf{n}$ is the outward normal vector at boundaries, $c_1^{\text{inj}}$ is the injected acid concentration (i.e. $H^+$ molar concentration) at the inlet and $R(c_1)$ is the reaction rate at the fracture wall faces.

At the inlet, the acid fluid with a specific acid concentration $c_1^{\text{inj}}$ is injected. The zero gradient boundary condition is defined at the outlet, top and bottom faces. At the fracture faces, the amount of $H^+$ transported to the fracture face is consumed by dissolving the calcite mineral.

The reaction rate between calcite ($CaCO_3$) and HCl is described by a linear rate law

$$R(c_1) = k c_1 \tag{10}$$

where $k$ is the reaction rate constant.

The initial condition needs to be given to complete the acid transport model.

$$c_1(t = 0) = c_1^0 \tag{11}$$

where $c_1^0$ is the initial molar concentration of $H^+$.

**Polymer Transport Model**

The concentration of the polymer in the aqueous solution is in weight percentage which is denoted by wt%. The polymer transport is modeled by the following advection-diffusion equation

$$\frac{\partial c_2}{\partial t} + \nabla \cdot (\mathbf{u} c_2) - \nabla \cdot (\mathbf{D}_2 \nabla c_2) = 0 \tag{12}$$

where $c_2$ is the mass fraction of the polymer and $D_2$ is the polymer diffusion-dispersion coefficient.

The boundary conditions of the polymer transport model are described as below.

$$(\mathbf{u} c_2 - \mathbf{D}_2 \nabla c_2) \cdot \mathbf{n} = (\mathbf{u}_{\text{inj}} \cdot \mathbf{n}) c_2^{\text{inj}} \quad \text{inlet face} \tag{13}$$

$$-\mathbf{D}_2 \nabla c_2 \cdot \mathbf{n} = 0 \quad \text{outlet/top/bottom/fracture wall faces} \tag{14}$$

where $c_2^{\text{inj}}$ is the injected polymer mass fraction at the inlet.

In this paper, $c_2^{\text{inj}} = 0$ since no polymer is injected at the inlet. The zero gradient boundary condition for $c_2$ is defined at other faces.

The initial condition needs to be given to complete the polymer transport model.

$$c_2(t=0) = c_2^0 \tag{15}$$

where $c_2^0$ is the initial polymer concentration.

**Acid Etching Model**

Since the acid dissolves the calcite mineral at the fracture surface, the domain of the fracture will be enlarged accordingly. The mesh motion is governed by the solid conservation equation.

$$c_s \frac{d\mathbf{r}}{dt} = \alpha R(c_1)\mathbf{n} \tag{16}$$

where $c_s$ is the molar density of the calcite mineral, $\mathbf{r}$ is the point vector on the fracture surfaces, and $\alpha$ is the stoichiometric conversion coefficient, defined as moles of calcite dissolved per mole of acid reacted. The $\alpha$ is 0.5 for the dissolution reaction between HCl and $CaCO_3$.

**Polymer Viscosity Model**

Here we assume that the viscosity of the polymer solution is a function of polymer concentration $c_2$. The effects of non-Newtonian behavior and salinity are not considered here. Our polymer viscosity model is modified from the Flory-Hugging equation[24].

$$\mu = \mu_w[1 + A_1 c_2 + A_2 c_2^2 + A_3 c_2^3] \tag{17}$$

where $\mu_w$ is the water viscosity, $A_1$, $A_2$ and $A_3$ are model parameters obtained from fitting the experimental data.

**Algorithm for Solving the Coupled System**

The solution algorithm is presented in **Fig. 7**. For each time step, the Navier-Stokes flow is solved first. The acid transport and polymer transport are then solved based on the new velocity field. The new acid concentration field is used to compute the amount of mineral dissolution. The fracture geometry is updated accordingly. The fluid viscosity is updated using the new polymer concentration field. This process is repeated until the final time.

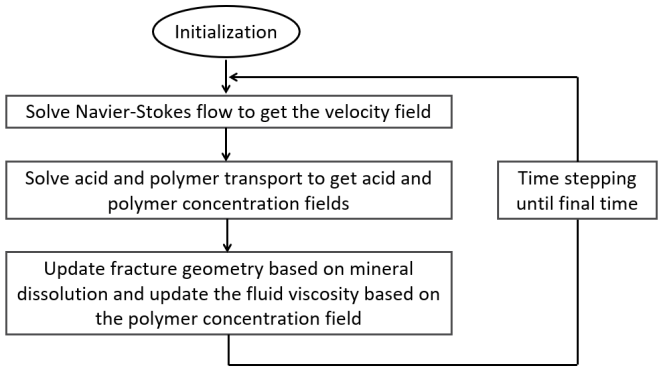


**Figure 7: Solution algorithm flowchart**

## Results

In this section, we conducted numerical simulations based on the developed 3D acid transport model to study the acid etching process in the fracture. We investigated acid etching in (1) vertical well acid fracturing treatments and (2) multistage acid fracturing treatments. We also analyzed the effects of perforation design and pad fluid viscosity on acid etching in multistage acid fracturing treatments.

### Acid Etching in Vertical Well Acid Fracturing Treatments

The purpose of modeling acid fracturing treatments in vertical wells is to compare acid etching processes under linear and radial flow conditions. A modeling study specifically for acid fracturing in vertical wells was presented in our previous paper [25]. In this study, the fracture size is at the lab scale. The initial fracture domain in a vertical well is illustrated in **Fig. 8**. The acid is injected through a perforation zone in the middle of the inlet boundary. The length and the width of the perforation zone are 0.2 cm and 0.1 cm respectively. Two cases are set up in order to study the effect of viscous fingering on acid etching in the fracture. The only difference between two cases is the type of pad fluid. The pad fluid of the first case is water (i.e. $c_2^0 = 0$) while the pad fluid is a 0.2422 wt% polymer solution (i.e. $c_2^0 = 0.2422$) in the second case. The initial viscosity of polymer solution, denoted by $\mu^0$, in the second case is 50 cP. **Fig. 9** shows how the polymer fluid viscosity changes with the polymer concentration, which is characterized by **Eq. 17**. The injected acid is a 10 wt% HCl solution. The input data for the numerical simulations is shown in **Table 1**. The final time for both cases is 11 minutes. Since the inertia effect is not obvious in this setup, the inertia term is dropped from **Eq. 1**.

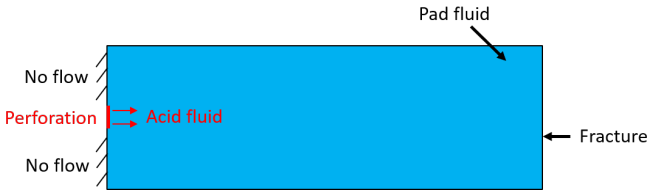


**Figure 8: Initial fracture domain in a vertical well**

**Table 1: Input data for numerical simulations**

| Parameter | Symbol | Units | Value |
|---|---|---|---|
| Fracture length | L | cm | 9 |
| Fracture height | H | cm | 3.14 |
| Fracture width | W | cm | 0.1 |
| Kinetic reaction rate constant | $k$ | cm/s | 0.15 |
| Acid diffusion coefficient | $D_1$ | $cm^2/s$ | 2.5e-5 |
| Injection velocity | $u_{inj}$ | cm/s | 0.5 |
| Water viscosity | $\mu_w$ | cP | 1 |
| Polymer viscosity model parameter | $A_1$ | - | 35 |
| Polymer viscosity model parameter | $A_2$ | - | 435 |
| Polymer viscosity model parameter | $A_3$ | - | 1055 |
| Water density | $\rho_w$ | $g/cm^3$ | 1 |
| Injected acid concentration | $c_1^{inj}$ | mol/L | 2.74 |
| Calcite rock molar concentration | $c_s$ | mol/L | 27 |

#### *Case 1: pad is water*

In this case, the pad fluid is water. The fluid viscosity does not change along the acid injection. The field of fracture width after acid etching is shown in **Fig. 10**. The simulation result shows that most of the

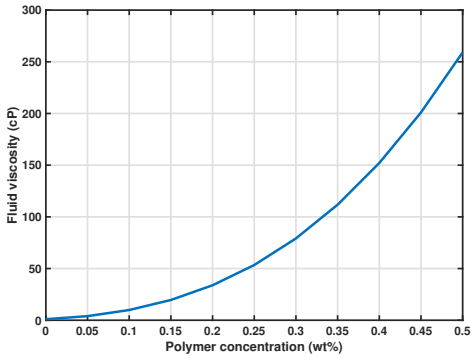


**Figure 9: Polymer fluid viscosity as a function of polymer concentration**

acid is spent near the fracture inlet. The increase in the fracture width is limited near the inlet. The etched fracture length is relatively short. Most of the fracture is left un-etched and will be closed after the acid injection. The overall acid fracture conductivity in this case is expected to be low.


**Figure 10: Field of fracture width in vertical well acid fracturing treatments (pad is water)**

### *Case 2: pad is polymer*

In this case, the pad fluid is a polymer solution. The fluid viscosity changes when injecting the acid. The field of fracture width after acid etching is shown in **Fig. 11**. A contour line of 1.2 mm fracture width is plotted to track the acid etching front. Acid etching fronts at the final time are compared between two cases: (1) the case where pad is water and (2) the case where pad is polymer. The comparison is shown in **Fig. 12**. In the case with polymer as the pad fluid, a high-conductivity channel develops in the middle of the fracture due to differential acid etching. Compared to the case without polymer, the etched fracture length is longer and the overall acid fracture conductivity should be higher in this case.


**Figure 11: Field of fracture width in vertical well acid fracturing treatments (pad is polymer)**

The difference in the acid etching patterns from the two cases is caused by the effect of the viscous fingering phenomenon. Streamlines have been computed on the middle slice of the fracture to show the fluid velocity field during acid etching. The velocity fields from the two cases at t = 33 s are shown in **Fig. 13** and **Fig. 14** respectively. The velocity field in Case 1 (pad is water) is more uniform than that in Case 2 (pad is polymer). In Case 2, there is a high-velocity zone in the middle of the fracture.

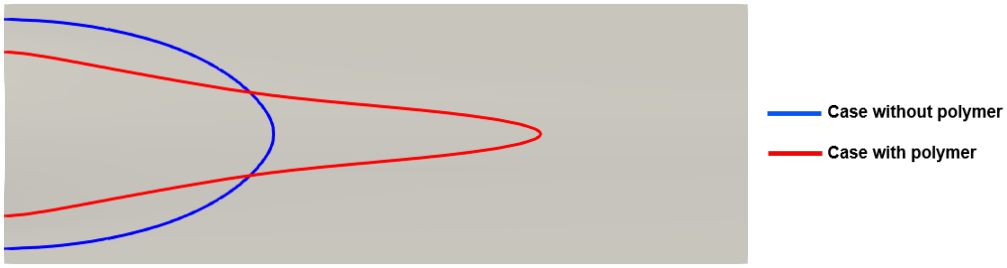


Figure 12: Comparison of acid etching fronts between Case 1 and Case 2 in vertical well acid fracturing

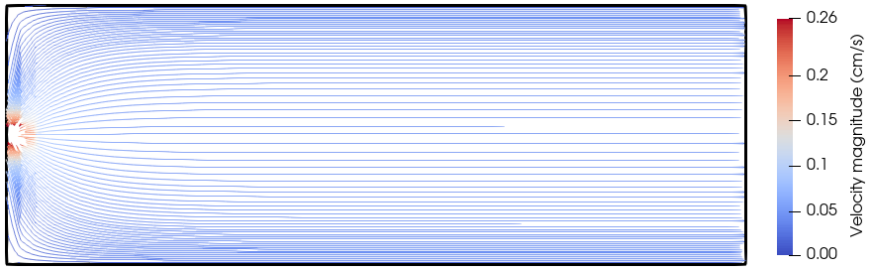


Figure 13: Velocity field in vertical well acid fracturing treatments (pad is water)

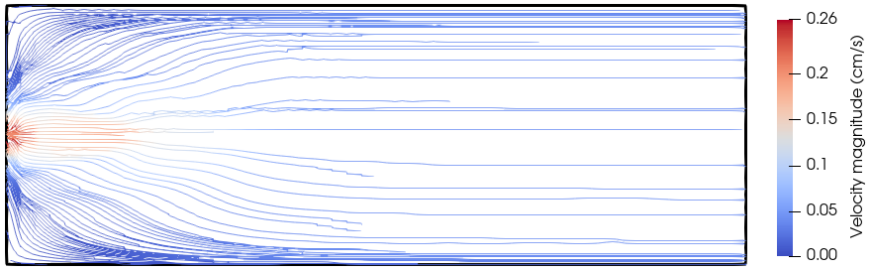


Figure 14: Velocity field in vertical well acid fracturing treatments (pad is polymer)

Acid concentration fields of Case 1 and Case 2 at t = 33 s are shown in **Fig. 15** and **Fig. 16** respectively. Acid concentration fields are always plotted on the middle slice of the fracture in this paper by default. In Case 2, acid is transported along a preferential flow path to etch the fracture surface in the fingering area. Since acid concentration dictates acid etching, the acid viscous fingering leads to non-uniform etching in Case 2.


Figure 15: Acid concentration in vertical well acid fracturing treatments (pad is water)

The velocity field in the fracture is largely dependent on the fluid viscosity field. The non-uniform velocity field in Case 2 results from the non-uniform viscosity field in Case 2. The viscosity field of Case 2 at t = 33 s is shown in **Fig. 17**. Early in the process of acid injection, the acid is injected through the perforation zone in the middle of the inlet. Since the acid viscosity is smaller than the polymer viscosity, the fluid viscosity in the mixing zone is smaller than the surrounding polymer fluid. The initial viscous fingering is triggered by the localized injection at the perforation. The velocity magnitude is larger in


**Figure 16: Acid concentration in vertical well acid fracturing treatments (pad is polymer)**

the fingering regions. More acid is diverted into the fingering region because fluid tends to flow into the less viscous area, which makes acid viscous fingering a positive feedback process. Since most acid flows along the center line of the fracture, more calcite is dissolved in the middle of the fracture, leading to the formation of the channel. The middle channel will be kept open after acid injection even under the closure stress of the formation. When compared to Case 1, the acid viscous fingering phenomenon enhances non-uniform acid etching near the fingering region, which is also consistent with previous experimental studies [11, 12].


**Figure 17: Viscosity field in vertical well acid fracturing treatments (pad is polymer)**

## Acid Etching in Multistage Acid Fracturing Treatments

In this section, we model acid etching process in multistage acid fracturing treatments. The initial transverse fracture domain is shown in **Fig. 18**. Here we assume that the transverse fracture is symmetric with respect to its diameter. Therefore we can model only one half of the transverse fracture to save some computational costs. The radius of inlet face is 1 cm and the radius of outlet face is 10 cm. The acid is injected through a perforation zone in the middle of the inlet boundary. The arc length and the width of the perforation zone are 0.2 cm and 0.1 cm respectively. Two cases are set up in order to study the effect of viscous fingering on acid etching in multistage acid fracturing treatments. In Case 1, pad is water while pad is polymer in Case 2. The final time for both cases is 66 minutes. The other input parameters are as the same as parameters of vertical well acid fracturing treatments in the previous section.

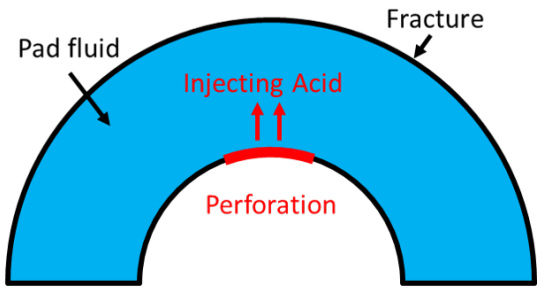


**Figure 18: Initial transverse fracture domain**

The fields of fracture width for Case 1 and Case 2 at the end of simulation are shown in **Fig. 19a** and **Fig. 19b** respectively. A contour line of 1.2 mm fracture width is plotted to track the acid etching front. The comparison of acid etching fronts between Case 1 and Case 2 is shown in **Fig. 20**. Acid etching is quite uniform in both Case 1 and Case 2. The etched area of Case 2 is slightly narrower than that of Case 1 because of the acid viscous fingering effect. With the current setup, we can not achieve non-uniform acid etching in multistage acid fracturing when pad is polymer.

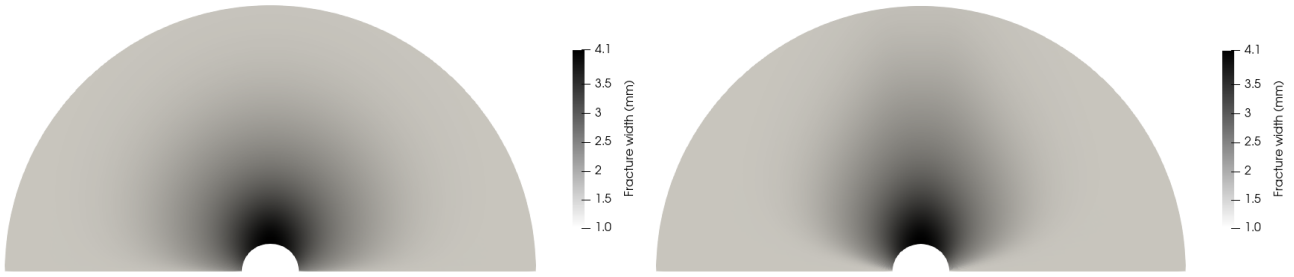


**(a) Case 1: pad is water** **(b) Case 2: pad is polymer**

**Figure 19: Field of fracture width in multistage acid fracturing treatments**

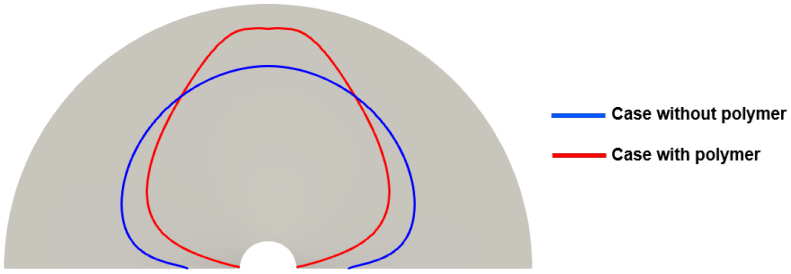


**Figure 20: Comparison of acid etching fronts between Case 1 and Case 2 in multistage acid fracturing**

The velocity fields of Case 1 and Case 2 at the final time are shown in **Fig. 21a** and **Fig. 21b** respectively. The velocity fields of both cases are quite uniform. The high velocity is only localized at the perforation zone. After the acid fluid is just injected through the perforation zone, the fluid flow quickly turns into a radial flow. The injection velocity is decomposed into many different directions and the velocity magnitude along each direction becomes much smaller than the magnitude of injection velocity. Therefore from the wellbore to the edge of the fracture, the high velocity at the perforation quickly dissipates and the overall velocity field becomes uniform. Compared with vertical well acid fracturing treatments, it is more difficult to achieve non-uniform acid etching in multistage acid fracturing treatments because the radial acid flow tends to make the velocity field uniform.

### Effect of Perforation Design on Multistage Acid Fracturing Treatments

For multistage acid fracturing treatments, it is necessary to introduce and maintain preferential flow paths in order to achieve non-uniform acid etching. In this section, we introduce a new perforation design and study the effect of perforation design on multistage acid fracturing treatments. The schematic of the new perforation design is shown in **Fig. 22**. Two perforations are added to the previous setup at the angles of 30°and 150°. Except the number of perforations, other input parameters are as the same as input parameters of the simulation illustrated in **Fig. 18**.

Similarly, two cases are simulated to study the acid etching with three perforations: (1) Case 1 where pad is water and (2) Case 2 where pad is polymer. The final time of simulation is 66 minutes. The simulation results of fracture width for Case 1 and Case 2 are shown in **Fig. 23a** and **Fig. 23b** respectively.

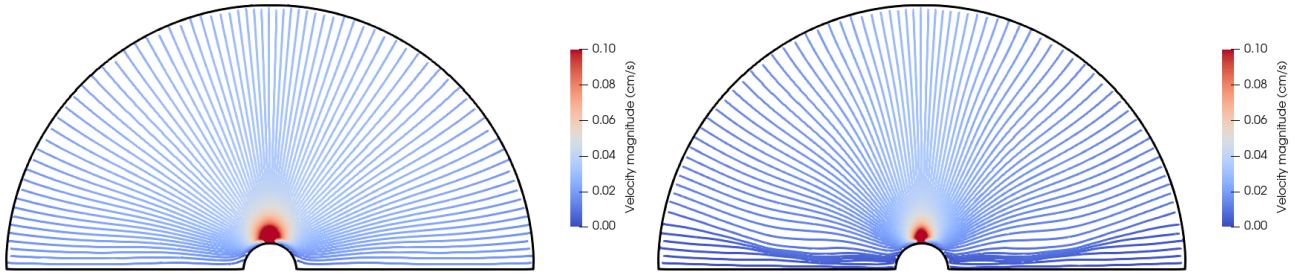


(a) Case 1: pad is water (b) Case 2: pad is polymer

**Figure 21: Velocity field in multistage acid fracturing treatments**

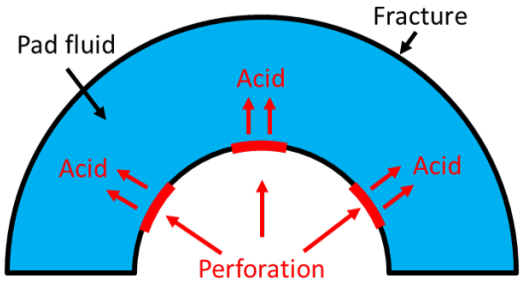


**Figure 22: Schematic of the transverse fracture domain with three perforations**

A contour line of 1.7 mm fracture width is plotted to track the acid etching front. The comparison of acid etching fronts between Case 1 and Case 2 is shown in **Fig. 24**. With these three perforations, non-uniform acid etching develops at each perforation in Case 2 while acid etching is still quite uniform in Case 1.

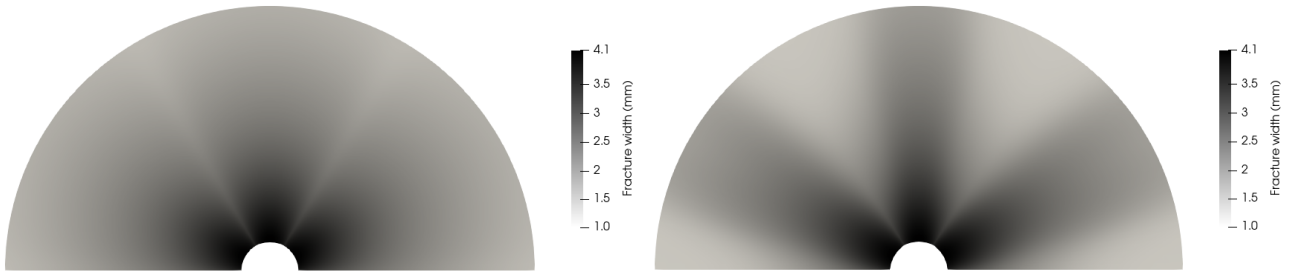


(a) Case 1: pad is water (b) Case 2: pad is polymer

**Figure 23: Field of fracture width in multistage acid fracturing treatments with three perforations**

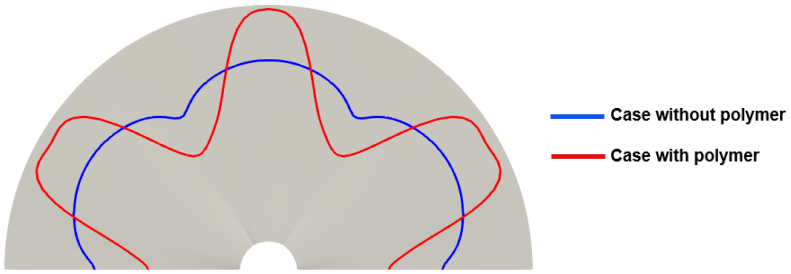


**Figure 24: Comparison of acid etching fronts between Case 1 and Case 2 in multistage acid fracturing with three perforations**

The velocity fields of Case 1 and Case 2 at the final time are shown in **Fig. 25a** and **Fig. 25b** respectively. In Case 2, three high-velocity regions form at three perforations and extend from the wellbore to

the edge of the transverse fracture. Most of the acid is transported along these three preferential flow paths, which leads to three acid-etched channels shown in **Fig. 24**. Compared with the velocity field of single perforation case shown in **Fig. 21b**, increasing the number of perforations helps prevent the injection velocity from being decomposed into smaller velocities along arbitrary directions near the wellbore face.

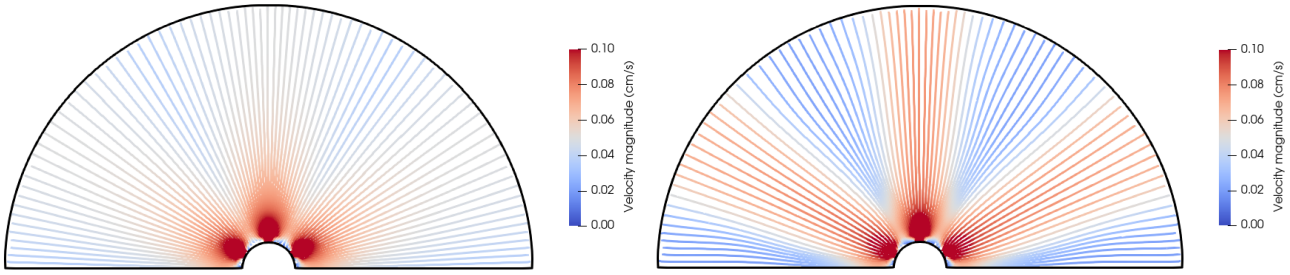


**(a) Case 1: pad is water** **(b) Case 2: pad is polymer**

**Figure 25: Velocity field in multistage acid fracturing treatments with three perforations**

Since acid etching is still uniform in Case 1 of this section as shown in **Fig. 24**, only increasing the number of perforations is not adequate to create non-uniform acid etching. It is the acid viscous fingering that develops preferential flow paths during the early period of multistage acid fracturing treatments. The viscosity field of Case 2 at t = 66 s is shown in **Fig. 26** while the viscosity is always water viscosity in Case 1. Velocity fields of Case 1 and Case 2 at t = 66 s are shown in **Fig. 27a** and **Fig. 27b** respectively. Simulation results show that acid viscous fingering leads to the growth of preferential flow paths. Therefore during the early period of multistage acid fracturing treatments, non-uniform acid etching is largely driven by acid viscous fingering.

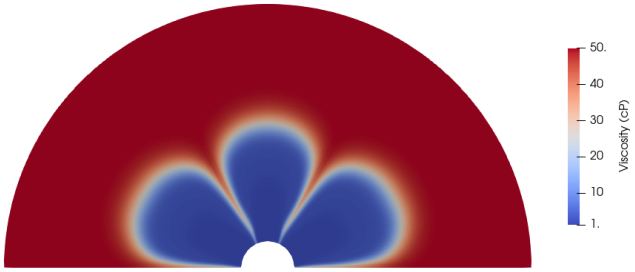


**Figure 26: Viscosity field of Case 2 in multistage acid fracturing treatments with three perforations (t = 66 s)**

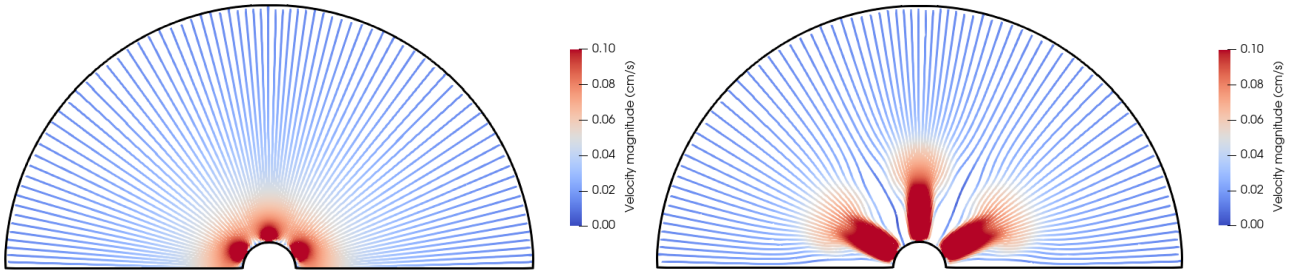


**(a) Case 1: pad is water** **(b) Case 2: pad is polymer**

**Figure 27: Velocity field in multistage acid fracturing treatments with three perforations (t = 66 s)**

Since polymer is removed from the transverse fracture at the outlet boundary, the viscosity field will become uniform after certain time. As shown in **Fig. 28**, the viscosity field is almost uniform at t = 30 min. Velocity fields of Case 1 and Case 2 at t = 30 min are shown in **Fig. 29a** and **Fig. 29b** respectively. Preferential flow paths in Case 2 is still maintained even though the viscosity field becomes uniform. This can be explained based on the field of fracture width as shown in **Fig. 30**. The blue line in **Fig. 30a** and the red line in **Fig. 30b** represent the contour line of 1.2 mm fracture width in Case 1 and Case 2 respectively. **Fig. 30b** shows that three channels with large fracture width have been created by non-uniform acid etching. Most of the acid will be transported into these channels and fracture width will keep increasing due to acid etching. After this point, the fracture roughness will drive the non-uniform acid etching. We can see that non-uniform acid etching itself is also a positive feedback process when there are some high-conductivity channels in the fracture.


**Figure 28: Viscosity field of Case 2 in multistage acid fracturing treatments with three perforations (t = 30 min)**

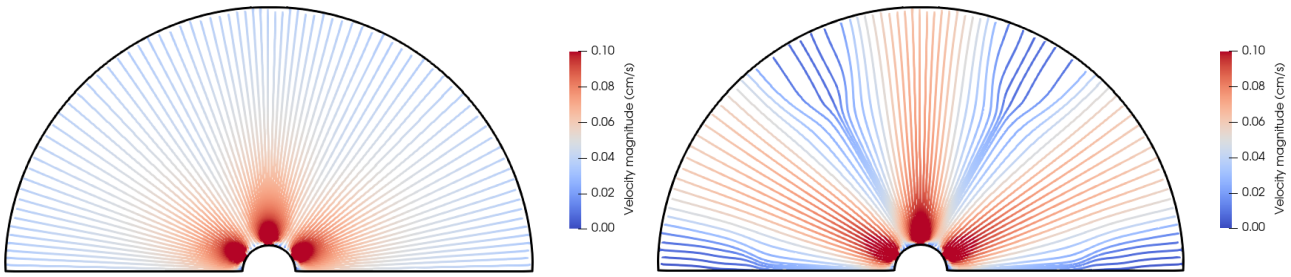


**(a) Case 1: pad is water** **(b) Case 2: pad is polymer**

**Figure 29: Velocity field in multistage acid fracturing treatments with three perforations (t = 30 min)**

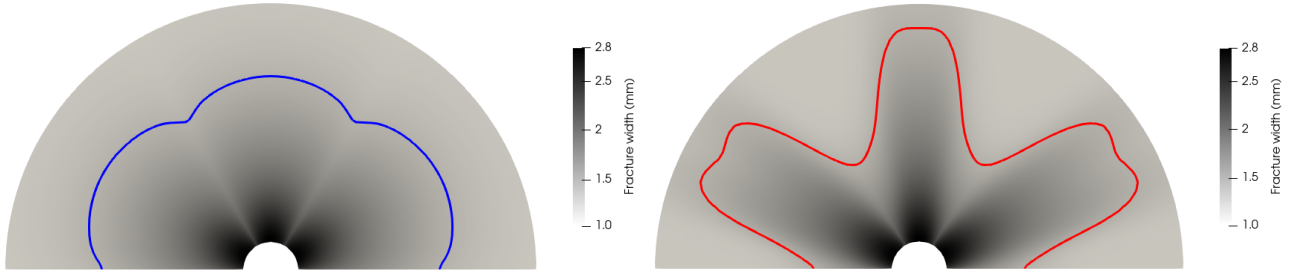


**(a) Case 1: pad is water** **(b) Case 2: pad is polymer**

**Figure 30: Field of fracture width in multistage acid fracturing treatments with three perforations (t = 30 min)**

### Effect of Pad Fluid Viscosity on Multistage Acid Fracturing Treatments

In this section, we investigate the effect of pad fluid viscosity on multistage acid fracturing treatments. The same input parameters seen in **Table 1** are used. Three sets of simulations were conducted with three different polymer viscosity values which are 50 cP, 100 cP and 200 cP. Contour lines of 2 mm fracture width in these three cases at t = 60 min are compared and shown in **Fig. 31**. As the pad fluid viscosity increases, the acid-etched channels becomes narrower and longer. Acid fracturing treatments usually favor a narrow channel over a wide channel because a narrow channel is less likely to collapse under the fracture closure stress [11]. The length of etched fracture also affects the effectiveness of acid fracturing treatments. A longer etched fracture tends to stimulate a larger volume of reservoir and usually results in a successful acid fracturing job.

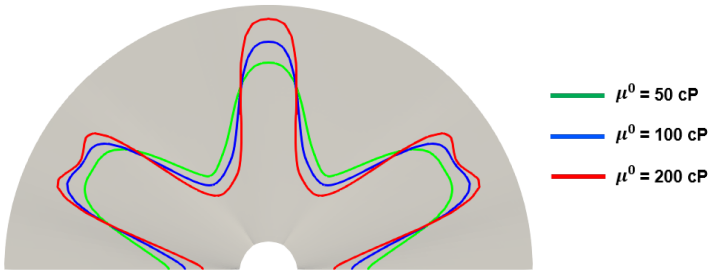


**Figure 31: Comparison of acid etching fronts in three cases with different pad fluid viscosities: (1) $\mu^0$ = 50 cP, (2) $\mu^0$ = 100 cP and (3) $\mu^0$ = 200 cP**

This trend can be explained by comparing the process of acid viscous fingering in these three cases. Velocity fields of these three cases at t = 2 min are shown in **Fig. 32**. Even though the patterns of viscous fingering look similar in these three cases, the area of viscous fingers and the velocity inside viscous fingers are different among three cases. When the viscosity contrast between pad and acid becomes larger, the area of acid viscous fingering becomes narrower. Narrow viscous fingers reduce the acid transport along the tangential direction so that the growth of acid-etched area is limited along the tangential direction. At the same time, the velocity magnitude in the viscous fingering area increases as the pad viscosity increases from 50 cP to 200 cP. With a large velocity in the viscous fingering area, the acid can be transported deep into the fracture. That's why the acid-etched fracture is longest when the pad viscosity is 200 cP. We anticipate that this trend may reach a plateau after the pad viscosity is larger than a threshold based on the theory of viscous fingering phenomenon. Our current study modeled the fluid viscosity as a function of polymer concentration. The non-Newtonian behavior of the polymer fluid such as shear thinning will be considered in the future work.

## Conclusions

This paper presents a mathematical model for multistage acid fracturing treatments with acid viscous fingering. Our model accounts for the processes of fluid flow, acid transport, polymer transport and fracture dissolution in the fracture. A numerical simulator has been developed to solve the coupled system. The fracture geometry can be obtained at the end of the acid injection period. We modeled vertical well acid fracturing treatments and multistage acid fracturing treatments. For both types of acid fracturing treatments, we compared the acid etching performance in two cases through numerical simulations: (1) where the pad fluid is polymer, and (2) where the pad fluid is water. Our simulation results showed that acid viscous fingering helps achieve non-uniform acid etching, which is also consistent with acid fracturing experiments in the literature. There are two mechanisms contributing to non-uniform acid etching: (1) viscous fingering at the early stage and (2) fracture roughness at the later stage. During the early period of acid injection, the viscous fingering phenomenon leads to a non-uniform velocity field. The acid is mostly transported to the fingering area. The acid etching activities are constrained in the fingering

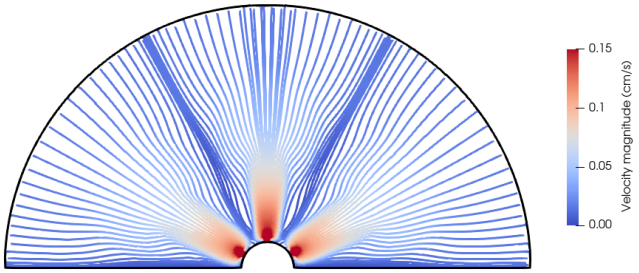


(a) Case 1: $\mu^0$ = 50 cP

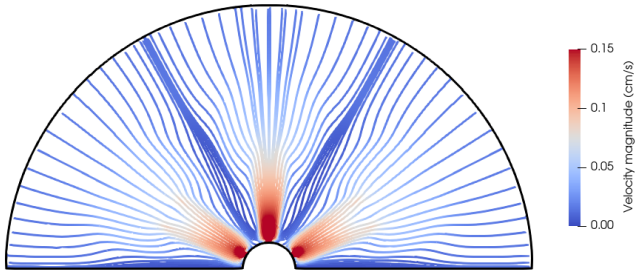


(b) Case 2: $\mu^0$ = 100 cP

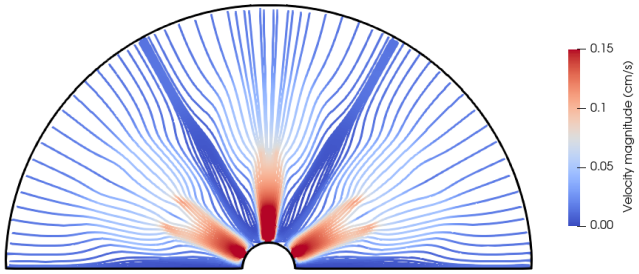


(c) Case 3: $\mu^0$ = 200 cP

**Figure 32: Velocity fields in multistage acid fracturing treatments with different pad viscosities (t = 2 min)**

regions, which results in high-conductivity channels and leaves other parts of the rock not etched. The viscous fingering effect gradually becomes weaker when the fluid viscosity field becomes more uniform. Afterwards the fracture roughness keeps developing non-uniform etching as most of the acid is diverted into high-conductivity channels which have been generated at the early stage. We found that it is more difficult to develop non-uniform acid etching in multistage acid fracturing treatments because the velocity field tends to be more uniform under the radial flow. To develop non-uniform etching in multistage acid fracturing treatments, we increased the number of perforations so that preferential flow paths can grow and be maintained during acid injection. We investigated the effect of the pad fluid viscosity on multistage acid fracturing treatments. Within current range of polymer viscosities investigated, the etched fracture length increases with an increasing pad viscosity. The high-conductivity channels becomes narrower when the pad viscosity increases. The developed model can be adopted to assist engineering designs by quantifying effects of various geologic and engineering parameters on acid fracturing treatments.

## Acknowledgements

This work was supported by the donors of the American Chemical Society Petroleum Research Fund (Grant #: 59356-ND9).

## Nomenclature

$\rho =$ fluid density
$\mathbf{u} =$ fluid velocity
$p =$ fluid pressure
$\mu =$ fluid viscosity
$c =$ concentration of components
$\mathbf{D} =$ diffusion-dispersion coefficient of components
$\mathbf{n} =$ outward normal vector at boundaries
$R =$ reaction rate
$k =$ kinetic reaction rate constant
$\mathbf{r} =$ point vector on fracture surfaces
$\alpha =$ stoichiometric conversion coefficient
$A_1, A_2, A_3 =$ model parameters in polymer viscosity model

## Subscripts

$1 =$ acid component
$2 =$ polymer component
$w =$ aqueous phase
$s =$ calcite rock
$\text{inj} =$ inlet boundary
$\text{out} =$ outlet boundary

## Superscripts

$0 =$ initial condition
$\text{inj} =$ inlet boundary

## References

[1] M. J. Economides, K. G. Nolte, Reservoir Stimulation, Prentice Hall Englewood Cliffs, NJ, 1989.

[2] D. McDuff, C. E. Shuchart, S. Jackson, D. Postl, J. S. Brown, Understanding wormholes in carbonates: Unprecedented experimental scale and 3-d visualization, in: SPE Annual Technical Conference and Exhibition, Society of Petroleum Engineers, 2010.

[3] R. Dong, S. Lee, M. Wheeler, Numerical simulation of matrix acidizing in fractured carbonate reservoirs using adaptive enriched Galerkin method, in: SPE Reservoir Simulation Conference, Society of Petroleum Engineers, 2019.

[4] R. Dong, Q. Wang, M. F. Wheeler, Prediction of mechanical stability of acidizing-induced wormholes through coupled hydro-chemo-mechanical simulation, in: 53rd US Rock Mechanics/Geomechanics Symposium, American Rock Mechanics Association, 2019.

[5] O. Al-Hinai, R. Dong, S. Srinivasan, M. F. Wheeler, A new equi-dimensional fracture model using polyhedral cells for microseismic data sets, Journal of Petroleum Science and Engineering 154 (2017) 49–59.

[6] M. Rafie, R. Said, M. Al-Hajri, T. Almubarak, A. Al-Thiyabi, I. Nugraha, E. Soriano, J. Lucado, The first successful multistage acid frac of an oil producer in Saudi Arabia, in: SPE Saudi Arabia Section Technical Symposium and Exhibition, Society of Petroleum Engineers, 2014.

[7] M. Mofti, L. Sierra, A. S. F. Alboueshi, N. Hadi Al-Azmi, S. Matar, A. Abu-Eida, M. Patra, Application of multistage acid fracturing to stimulate mishref carbonate formation: Case study, minagish field, west kuwait, in: Abu Dhabi International Petroleum Exhibition & Conference, Society of Petroleum Engineers, 2019.

[8] J. M. Petriz Munguia, B. E. Gonzalez Valtierra, J. Trujillo Hernandez, S. Santos, K. Campos Monroy, Acid-fracturing techniques as a good alternative to help improve field development assets, in: Abu Dhabi International Petroleum Exhibition & Conference, Society of Petroleum Engineers, 2019.

[9] P. Zhao, R. Dong, Y. Liang, Regional to local machine-learning analysis for unconventional formation reserve estimation: Eagle Ford case study, in: SPE Annual Technical Conference and Exhibition, Society of Petroleum Engineers, 2020.

[10] J. Mou, D. Zhu, A. D. Hill, Acid-etched channels in heterogeneous carbonates–a newly discovered mechanism for creating acid-fracture conductivity, SPE Journal 15 (02) (2010) 404–416.

[11] D. Davies, M. Bosma, W. De Vries, Development of field design rules for viscous fingering in acid fracturing treatments: A large-scale model study, in: Middle East Oil Show, Society of Petroleum Engineers, 1987.

[12] X. Li, Y. Chen, Z. Yang, F. Chen, Large-scale visual experiment and numerical simulation of acid fingering during carbonate acid fracturing, in: SPE/IATMI Asia Pacific Oil & Gas Conference and Exhibition, Society of Petroleum Engineers, 2017.

[13] K. Ben-Naceur, M. J. Economides, Design and evaluation of acid fracturing treatments, in: Low Permeability Reservoirs Symposium, Society of Petroleum Engineers, 1989.

[14] E. Koval, A method for predicting the performance of unstable miscible displacement in heterogeneous media, Society of Petroleum Engineers Journal 3 (02) (1963) 145–154.

[15] R. Gdanski, W. Lee, On the design of fracture acidizing treatments, in: SPE Production Operations Symposium, Society of Petroleum Engineers, 1989.

[16] K. Lo, R. Dean, Modeling of acid fracturing, SPE Production Engineering 4 (02) (1989) 194–200.

[17] A. Settari, Modeling of acid-fracturing treatments, SPE Production & Facilities 8 (01) (1993) 30–38.

[18] A. Settari, R. Sullivan, C. Hansen, A new two-dimensional model for acid fracturing design, in: SPE Annual Technical Conference and Exhibition, Society of Petroleum Engineers, 1998.

[19] J. Romero, H. Gu, S. Gulrajani, 3d transport in acid-fracturing treatments: Theoretical development and consequences for hydrocarbon production, SPE Production & Facilities 16 (02) (2001) 122–130.

[20] V. Starchenko, C. J. Marra, A. J. Ladd, Three-dimensional simulations of fracture dissolution, Journal of Geophysical Research: Solid Earth 121 (9) (2016) 6421–6444.

[21] OpenFOAM website, https://www.openfoam.com/.

[22] V. Starchenko, A. J. Ladd, The development of wormholes in laboratory-scale fractures: Perspectives from three-dimensional simulations, Water Resources Research 54 (10) (2018) 7946–7959.

[23] M. Anderson, S. Fredrickson, Dynamic etching tests aid fracture-acidizing treatment design, SPE Production Engineering 4 (04) (1989) 443–449.

[24] P. J. Flory, Principles of polymer chemistry, Cornell University Press, 1953.

[25] R. Dong, M. F. Wheeler, K. Ma, H. Su, A 3D acid transport model for acid fracturing treatments with viscous fingering, in: SPE Annual Technical Conference and Exhibition, Society of Petroleum Engineers, 2020.